Theor Chem Acc (2014) 133:1450
DOI 10.1007/s00214-014-1450-4

REGULAR ARTICLE

Unimolecular and hydrolysis channels for the detachment of water from microsolvated alkaline earth dication (Mg^{2+}, Ca^{2+}, Sr^{2+}, Ba^{2+}) clusters

Evangelos Miliordos · Sotiris S. Xantheas

Received: 29 October 2013 / Accepted: 11 January 2014 / Published online: 7 February 2014

Abstract We examine theoretically the three channels that are associated with the detachment of a single water molecule from the aqueous clusters of the alkaline earth dications, $[M(H_2O)_n]^{2+}$, M = Mg, Ca, Sr, Ba, $n \leq 6$. These are the unimolecular water loss ($M^{2+}(H_2O)_{n-1} + H_2O$) and the two hydrolysis channels resulting the loss of hydronium ($[MOH(H_2O)_{n-2}]^+ + H_3O^+$) and Zundel ($[MOH(H_2O)_{n-3}]^+ + H_3O^+(H_2O)$) cations. Minimum energy paths (MEPs) corresponding to those three channels were constructed at the Møller–Plesset second order perturbation (MP2) level of theory with basis sets of double- and triple-ζ quality. We furthermore investigated the water and hydronium loss channels from the mono-hydroxide water clusters with up to four water molecules, $[MOH(H_2O)_n]^+$, $1 \leq n \leq 4$. Our results indicate the preference of the hydronium loss and possibly the Zundel-cation loss channels for the smallest size clusters, whereas the unimolecular water loss channel is preferred for the larger ones as well as the mono-hydroxide clusters. Although the charge separation (hydronium and Zundel-cation loss) channels produce more stable products when compared to the ones for the unimolecular water loss, they also require the surmounting of high-energy barriers, a fact that makes the experimental observation of fragments related to these hydrolysis channels difficult.

Keywords Alkaline earth dication aqueous clusters · Unimolecular dissociation · Potential energy curve · Electronic structure · Hydrolysis channel

1 Introduction

The structure and stability of small aqueous clusters of alkaline earth metal dications (Mg^{2+}, Ca^{2+}, Sr^{2+}, and Ba^{2+}) has been the subject of numerous experimental [1–18] and theoretical [4, 8, 11, 14–36] studies aimed at providing archetypal models for their aqueous solvation. It is generally accepted that the first solvation shell of these ions in water is saturated with six water molecules [6, 10, 11, 13, 14]. The speciation of these metal cations in an aqueous environment depends both upon their electronic properties as well as the characteristics of the aqueous environment [37]. The second ionization potential (IP) of the alkaline earth metals (save Mg) [38] is below the first ($^2B_1$) IP of water (12.6206 ± 0.0020 eV) [39], and this determines the position of the lower asymptote that correlates with the formation of the aqueous complex [36]. Depending on the pH of an aqueous solution, the speciation ranges [37] from $M^{2+}(H_2O)_n$ to $[M_x(OH)_y]^{(2x-y)+}$, M = Mg, Ca, Sr or Ba. The following two channels:

$$M^{2+}(H_2O)_n \rightarrow \left[M(H_2O)_{n-1}\right]^{2+} + H_2O \quad (1)$$

$$M^{2+}(H_2O)_n \rightarrow \left[MOH(H_2O)_{n-2}\right]^{+} + H_3O^{+} \quad (2)$$

describe the unimolecular dissociation and hydrolysis mechanisms, respectively. The first one corresponds to the process of pure water loss originating from the exchange of

Dedicated to Professor Thom Dunning and published as part of the special collection of articles celebrating his career upon his retirement.

Electronic supplementary material The online version of this article (doi:10.1007/s00214-014-1450-4) contains supplementary material, which is available to authorized users.

E. Miliordos · S. S. Xantheas (✉)
Physical Sciences Division, Pacific Northwest National Laboratory, 902 Battelle Boulevard,
P.O. Box 999, MS K1-83, Richland, WA 99352, USA
e-mail: sotiris.xantheas@pnnl.gov

ligands between the first and second solvation shells, whereas the second one is usually referred to as the charge separation reaction in the literature. In the latter case, the escaping water molecule initially creates a hydrogen bond with one of the other water molecules attached to the metal in the first solvation shell and subsequently detaches a H^+ ion from one of the first shell ligands producing H_3O^+. In the following, we will refer to this second channel as the one corresponding to the loss of hydronium. The remaining singly charged metal hydroxide cluster and hydronium fragments experience Coulombic repulsion and can break apart [11, 14, 16, 17, 29]. It has been demonstrated that the net charge on the metal remains practically unchanged revealing a bonding picture of the type [24, 29] $M^{2+}(H_2O)_m(OH^-)$. It should be mentioned that the charge separation pathway has been observed experimentally only for the lighter metal clusters [1, 6, 7, 12]. For instance, the $[Ca(H_2O)]^{2+}$ complex was elusive during collision-induced experiments until recently [16], due to the charge separation $[Ca(H_2O)]^{2+} + H_2O \rightarrow CaOH^+ + H_3O^+$ reaction [1, 12]. Similarly, the largest cluster size for which this reaction has been reported to occur [7] is four water molecules for Mg and two for the other three metals.

Experimentally, doubly charged aqueous clusters of the alkaline earth metal ions were produced by electrospray ionization, and special effort has been devoted to the measurement of their hydration energies. To this end, Armentrout and co-workers have recently employed the collision-induced dissociation (CID) combined with the guided ion beam tandem mass spectrometry techniques to study the aqueous clusters of Mg, Ca, and Sr [11, 14, 16, 17]. CID was also used by Barran et al. [6] to examine the Mg clusters, while Williams and co-workers applied the blackbody infrared dissociation (BIRD) methodology to study the aqueous clusters of all four metals [5, 9]. Finally, Kerbale and co-workers used high-pressure mass spectrometry (HPMS) to also study clusters of all four metal dications [2, 3].

From the theoretical point of view, most of the previous calculations have been reported using the density functional theory (DFT) with a variety of functionals and basis sets [8, 11, 14, 16, 17, 27–30, 33–35]. Ab initio results have been reported at the (restricted) Hartree–Fock (RHF) and Møller–Plesset second order perturbation (MP2) levels of theory [4, 8, 11, 16, 17, 19–21, 23–25, 31, 33, 35]. The previous theoretical results reported in the literature have mainly focused on obtaining the optimal geometries of the $[M(H_2O)_n]^{2+}$ clusters, including their various isomers, and their energies with emphasis in estimating their hydration energies. The majority of the previous studies have dealt with the clusters of the first two metal atoms, Ca and Mg [4, 8, 11, 16, 17, 19–21, 23, 25, 27–35], while considerably less attention has been paid to aqueous clusters of Sr [14, 19–21, 23, 29] and Ba [19, 23, 29] dications. The structures and hydration energies of the $[M(H_2O)_n(OH)]^+$ ions have also been reported in the literature for M = Mg, Ca, and Ba [18, 22, 26]. Finally, we would like to mention that only a handful of studies have previously theoretically examined the charge separation process described by reaction (2). Specifically, Beyer et al. [29] in 1999 studied both of the chemical reactions (1) and (2) for all four metals, while Peschke et al. [28] in the same year reported analogous results for the cases of Mg and Ca. In both articles, transition states and energy barriers were reported for clusters with just two water molecules. More than 10 years later, Armentrout and co-workers examined the stationary points (equilibrium structures and transition states) of the $[Mg(H_2O)_{3,4}]^{2+}$, $[Ca(H_2O)_{2,3}]^{2+}$, and $[Sr(H_2O)_2]^{2+}$ systems [14, 16, 17]. However, no minimum energy paths (MEPs) have yet been reported in the literature for those and larger clusters.

In the present study, we report the MEPs for the reactions (1) and (2), for all four alkaline earth metals with $n = 2, 3$ water molecules at the MP2 level of theory. For Mg, we additionally included the MEPs for $n = 4$. In the cases of $n = 3, 4$, we also constructed the MEPs relative to the following reaction, which involves the Zundel cation (Zundel-cation loss channel):

$$M^{2+}(H_2O)_n \rightarrow \left[MOH(H_2O)_{n-3}\right]^+ + H_3O^+(H_2O). \quad (3)$$

Reactions (2) and (3) can be both considered as charge separation processes. For $n > 4$, we report only the relative energetics of the reactants and products of reactions (1), (2), and (3). Furthermore, the full MEPs for the removal of one additional water molecule from the product $[M(H_2O)_m(OH)]^+$ cations for $m = 2$ are reported. We show that the water loss reaction prevails for this case, as the charge separation reaction leading to $M(OH)_2 + H_3O^+$ is not energetically favorable.

The article is organized as follows: In Sect. 2, we outline the computational methods used in the present study. In Sect. 3, we describe the MEPs for the $[M(H_2O)_n]^{2+}$ species, where M = Mg, Ca, Sr, Ba and $n = 2$, 3, or 4 (only for Mg). In Sect. 4, we present the results of the energetics of reactions (1–3) for all four metals up to six water molecules. Finally, in Sect. 5, we examine the water loss process of the $[M(H_2O)_{n-1}(OH)]^+$ species. Section 6 summarizes our findings.

2 Computational details

All calculations reported in this study were carried out at the Møller–Plesset second order perturbation level of theory (MP2). The 1*s* orbitals of oxygen and the 1*s*2*s*2*p* orbitals of Mg and Ca were kept frozen. We used two different

basis sets of double- and triple-ζ quality for H, O, Mg, and Ca. Specifically, for O and H, we used Dunning's aug-cc-pVDZ and aug-cc-pVTZ basis sets [40, 41], for Mg, the cc-pV(D + *d*)Z and cc-pV(T + *d*)Z [42], and for Ca, the cc-pVDZ and cc-pVTZ basis sets [43]. For Sr and Ba, we used the small-core relativistic pseudopotentials ECP28MDF and ECP46MDF, which replace the 1*s*2*s*2*p*3*s*3*p*3*d* and 1*s*2*s*2*p*3*s*3*p*3*d*4*s*4*p*4*d* electrons, respectively [44]. These pseudopotentials are combined with the 8*s*8*p*5*d*4*f* and 9*s*9*p*6*d*4*f* Gaussian functions to construct the molecular orbitals of the remaining electrons [44]. From now on, we use the acronyms ADZ and ATZ to denote the various basis sets as follows: ADZ = cc-pV(D + *d*)Z/(Mg), cc-pVDZ/(Ca), ECP28MDF-f/(Sr), ECP46MDF-f/(Ba), aug-cc-pVDZ/(O,H) and ATZ = cc-pV(T + *d*)Z/(Mg), cc-pVTZ/(Ca), ECP28MDF/(Sr), ECP46MDF/(Ba), aug-cc-pVTZ/(O,H).

All calculations, including the geometry optimizations, were performed with no symmetry constraints to exclude any artificially converged highly symmetric structures. To further verify that the located structures are real minima, we also calculated the harmonic vibrational frequencies at the equilibrium structures at the MP2/ADZ level. These structures compare very well with the ones already reported in the literature (when available). Zero-point energy (ZPE) corrections were estimated using these harmonic frequencies, i.e., no anharmonicities are included. For the frequencies, we used the atomic mass of the most abundant isotope, namely 1.00783 (^{1}H), 15.9949 (^{16}O), 23.98505 (^{24}Mg), 39.9626 (^{40}Ca), 87.9056 (^{88}Sr), and 137.905 (^{138}Ba). The MEPs as a function of the *R*(M–O) distance are obtained at the MP2/ADZ level of theory by optimizing the rest of the internal coordinates for each value of *R*. The MP2/ATZ//MP2/ADZ energetics of the various stationary points of the MEPs are used in the discussion of their features. All calculations were performed with the MOLPRO [45] and Gaussian09 [46] electronic structure codes.

3 Minimum energy paths of $[M(H_2O)_n]^{2+}$

In the following, we report the MEPs for the systems with the following stoichiometry: $[Mg(H_2O)_{2,3,4}]^{2+}$ (Sect. 3.1), $[Ca(H_2O)_{2,3}]^{2+}$ (Sect. 3.2), and $[Sr(H_2O)_{2,3}]^{2+}$, $[Ba(H_2O)_{2,3}]^{2+}$ (Sect. 3.3). All optimized structures, their energies, and harmonic vibrational frequencies are given in the Supporting Information.

3.1 $[Mg(H_2O)_{2,3,4}]^{2+}$

Figure 1 shows the MEPs at the MP2/ADZ level of theory for both the water loss and the charge separation channels of the $[Mg(H_2O)_2]^{2+}$ system. The MEP was constructed by

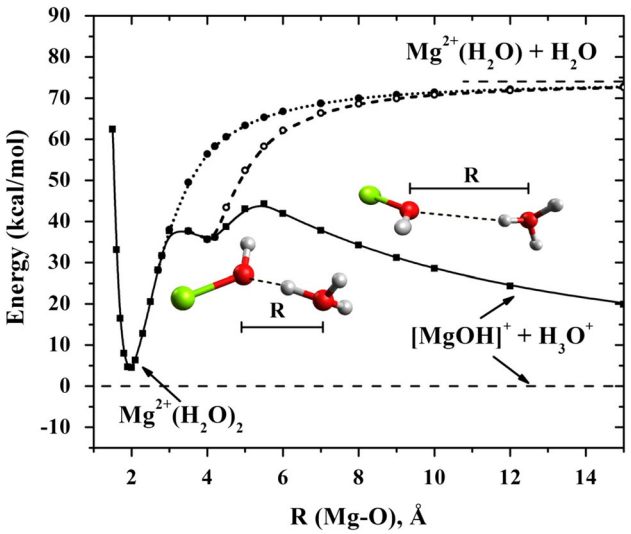

Fig. 1 Minimum energy paths of the $[Mg(H_2O)_2]^{2+}$ system

pulling one water molecule (bearing the O_1 atom) away from the ion and optimizing the rest of the geometrical parameters for every Mg–O_1 distance. Along the unimolecular water loss channel, this ligand can be detached either with or without making a hydrogen bond with the second water molecule. These two possibilities are shown in the MEP of Fig. 1: The dotted line with the solid circles for *R*(Mg–O) >3 Å traces the (higher energy) path along which no hydrogen bond is formed. On the other hand, there is a lower energy path for 3 Å < *R*(Mg–O_1) < 4 Å due to the formation of a hydrogen bond followed by an increase in the energy to the $[Mg(H_2O)]^{2+} + H_2O$ asymptote (dashed line with open circles in Fig. 1). This hydrogen-bonded minimum lies 31.4 kcal/mol higher in energy than the $Mg^{2+}(H_2O)_2$ global minimum; and it is stabilized with respect to that global minimum by a small barrier of 2.3 kcal/mol. By forcing the water molecule to be further detached from the ion, the charge separation channel [reaction (2)] opens up, facilitated by the loss of a H^+ ion from the first solvation shell. This MEP is shown with a solid line and filled square symbols in Fig. 1 (for *R*(Mg–O) >4 Å). Observe that the charge separation MEP is always lower in energy than the water loss MEPs. Moving from the H-bonded structure and after surmounting a barrier of 8.5 kcal/mol at *R*(Mg–O) ~5.5 Å, the charge separation MEP falls off as 1/*R* to the $MgOH^+ + H_3O^+$ asymptote due to Coulombic repulsion. Due to the 1/*R* dependence, even for a distance of *R*(Mg–O) ~15 Å, the energy is 20 kcal/mol higher than the asymptotic limit, which lies 4.7 kcal/mol lower than the energy of the $Mg^{2+}(H_2O)_2$ minimum.

Our MP2 relative energies compare favorably with the DFT values of Peschke et al. [28] and Beyer et al. [29]. In particular, relative to the equilibrium structure, our

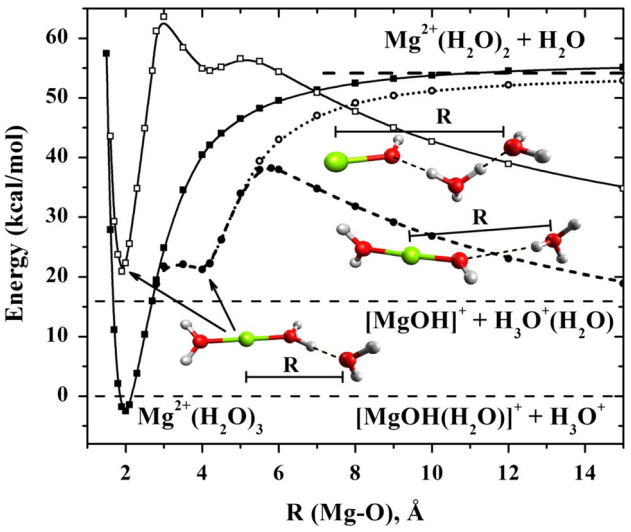

Fig. 2 Minimum energy paths of the $[Mg(H_2O)_3]^{2+}$ system. The *dashed line* with the *filled circles* dissociates to $[MgOH(H_2O)]^+ + H_3O^+$, whereas the *solid line* with the *open squares* to $[MgOH]^+ + H_3O^+(H_2O)$

H-bonded minimum is at 31.4 kcal/mol, whereas B3LYP gives a value of 31.5 kcal/mol [29]. The transition state of the charge separation reaction at $\sim$5.5 Å is presently at 39.9 kcal/mol, while B3LYP with two different basis sets gives 36.3 [28] and 39.4 kcal/mol [29], respectively. It should be mentioned that those DFT barriers included zero-point energy corrections (unlike ours, since we performed ZPE corrections only for the minima). To summarize, the lowest energy path for the detachment of a water molecule from the $Mg^{2+}(H_2O)_2$ minimum corresponds first to the formation of a hydrogen bond, $Mg^{2+}(H_2O)\ldots H_2O$ and then to the dissociation to $MgOH^+ + H_3O^+$, i.e., it starts off as a unimolecular water loss and ends up to the charge separated products.

We turn now to the $[Mg(H_2O)_3]^{2+}$ case and the corresponding MEPs shown in Fig. 2. In that case, we have three different adiabatic channels: (a) the water loss, reaction (1), (b) the hydronium loss, reaction (2), and (c) the Zundel-cation loss, reaction (3) channels. In the former two cases, the distance R of the x axis is measured from the Mg center to the oxygen atom of the departing water molecule, as in Fig. 1. In the latter case, we, however, measure the distance R from the Mg center to the oxygen atom of the Zundel cation further away from Mg. We would like to remind once again that all other geometrical parameters are optimized along the MEPs for every R(Mg–O) value without the use of any symmetry constraints.

We first describe the MEPs of Fig. 2 for the $[Mg(H_2O)_2]^{2+} + H_2O$ water loss channel starting from large R distances and moving down to the global minimum at R(Mg–O) $\sim$2 Å. As before, the water can approach the Mg^{2+} positively charged center by interacting or not with the rest of the water molecules. The solid line (filled squares) starting from the $Mg^{2+}(H_2O)_3$ equilibrium structure and ending in the $Mg^{2+}(H_2O)_2 + H_2O$ asymptote represents the path where there are no hydrogen bonds of the departing water with any of the other ligands. On the other hand, the formation of a H-bond makes the $[Mg(H_2O)_2]^{2+}\ldots H_2O$ attractive interaction more efficient, and thus, the respective MEP (dotted line, open circles) decreases faster going to the H-bonded shallow minimum at $\sim$4 Å. Pushing the water molecule of the second solvation shell further toward the metal center leads to the global $Mg^{2+}(H_2O)_3$ minimum via a negligible barrier.

For the lowest $[Mg(H_2O)(OH)]^+ + H_3O^+$ adiabatic path (dashed line, filled circles in Fig. 2), there is a Coulombic repulsion responsible for the $1/R$ shape of the MEP for R(Mg–O) >5.8 Å. At this distance, the positively charged hydronium experiences the negative local charge of the oxygen atom of the OH group. Recall that the $Mg^{2+}(H_2O)(OH^-)$ bonding picture has been previously suggested in the literature [24, 29]. At this point, one of the hydrogen atoms of H_3O^+ migrates to the oxygen of the OH group and the MEP turns over decreasing in energy. By the time the H atom has moved close to OH, we have the formation of a H-bond, and therefore, this path crosses the MEP coming from the $[Mg(H_2O)_2]^{2+} + H_2O$ channel (dotted line, open circles).

We finally examine the $MgOH^+ + H_3O^+(H_2O)$ channel which lies $\sim$15.8 kcal/mol higher than the $[Mg(H_2O)(OH)]^+ + H_3O^+$ asymptote. For reasons of clarity in Fig. 2, for this case, we show the MEP in terms of the distance R between the Mg center and the oxygen atom of the more distant water molecule. For long distances, we again observe the $1/R$ repulsive behavior (solid line, open squares). As the Zundel-cation approaches, the negative charge of OH is not screened anymore from the Mg^{2+} center, and one of its hydrogen atoms moves to the negatively charged OH group, as in the previous case. As a result, the cluster with two hydrogen bonds, schematically drawn as $Mg^{2+}(H_2O)\ldots(H_2O)\ldots(H_2O)$, is formed (this is the minimum located at $R = 4.2$ Å lying 54.6 kcal/mol above the lowest asymptote). By pushing further in the most distant water molecule, i.e., decreasing R, that molecule eventually is attached to Mg producing the $[Mg(H_2O)_2]^{2+}\ldots H_2O$ minimum (last ligand in the second solvation shell of the Mg center). Notice that now since R corresponds to the distance between Mg and the O of the first shell, the minimum is at $R = 1.9$ Å. This interaction is reported here for the first time in the literature.

In summary, removing a water molecule from the $[Mg(H_2O)_3]^{2+}$ minimum structure leads to the $[MgOH(H_2O)]^+ + H_3O^+$ fragments. This process is facilitated via

the formation of a hydrogen-bonded intermediate, and its subsequent decomposition over a barrier lying 23.7 and 40.7 kcal/mol above the $Mg^{2+}(H_2O)_3$ minimum, respectively. The corresponding numbers at the DFT [B3LYP/6-311 + G(2d,2p)//B3LYP/6-311 + G(d,p)] level, corrected for ZPE, are 22.5 and 38.7 kcal/mol [17], in good agreement with our present results. The dissociation energies for reactions (1–3) are 2.3, 18.5, 56.9 kcal/mol, respectively. Estimates of 0.2 and 55.2 kcal/mol for the first and third channels have been previously reported by Carl et al. [16].

We next consider the case with four water molecules. The corresponding MEPs are shown in Fig. 3, and they describe the same channels as the ones in Fig. 2 for the $n = 3$ case; in this respect, the MEPs of the two figures bear similar features. One difference is that the energy gaps between the first dissociation channel (hydronium loss) and the next two (Zundel cation and water loss) have now decreased appreciably from 15 and 55 kcal/mol for the $n = 3$ case, now being 5 and 35 kcal/mol, respectively. As a result, the MEPs for the $n = 4$ case are packed closer together than for $n = 3$. Along the channel that removes a water molecule from the $Mg^{2+}(H_2O)_4$ minimum, the hydrogen-bonded intermediate $[Mg(H_2O)_3]^{2+}\ldots H_2O$ at $R = 4$ Å and energy 7.7 kcal/mol (cf. Fig. 3) is initially formed. Compared to Fig. 2, the MEP leading to hydronium loss (dashed line with filled circles in Fig. 3) lies above the one leading to water loss (dotted line with open circles) for distances between 4 and 8 Å; this will certainly play an important role in the overall dynamics and kinetics of processes (1) and (2). Taking into account the Zundel-cation loss channel, which also passes through the above H-bonded structure, will further add to the complexity. The relative energetics of the several stationary points in Fig. 3 are within ~4 kcal/mol with the DFT results of Carl et al. [17].

A few interesting observations regarding the MEPs of $[Mg(H_2O)_n]^{2+}$, $n = 2, 3, 4$ (Figs. 1, 2, 3) are in order. First, the transition from the $Mg^{2+}(H_2O)_n$ to the $[Mg(H_2O)_{n-1}]^{2+}\ldots H_2O$ structure becomes easier with increasing n, since the energy difference decreases from 31.3, to 23.7, to 18.0 kcal/mol. In contrast, the barrier from $[Mg(H_2O)_{n-1}]^{2+}\ldots H_2O$ to $[Mg(H_2O)_{n-2}(OH)]^{2+}\ldots H_3O^+$ increases with n, from 8.7 ($n = 1$) to 17.0 ($n = 2$) to 28.7 ($n = 3$) kcal/mol. The MEPs of Figs. 1, 2, and 3 demonstrate the in situ formation of $[Mg(H_2O)_n]^{2+}$ from $[Mg(H_2O)_{n-1}]^{2+} + H_2O$. However, although the binding energy of the water molecule decreases with n mostly due to the increasing steric repulsion, the binding energy of the $Mg^{2+}(H_2O)_n$ global minimum with respect to the lowest energy fragments (hydronium loss asymptote) is increasing, from −4.5 ($n = 1$) to 2.5 ($n = 2$) to 10.3 ($n = 3$) kcal/mol, i.e., the hydrated metal cluster is becoming more stable with respect to the lowest dissociation asymptote.

3.2 $[Ca(H_2O)_{2,3}]^{2+}$

The MEPs of the $[Ca(H_2O)_2]^{2+}$ and $[Ca(H_2O)_3]^{2+}$ systems are shown in Figs. 4 and 5, respectively. We adopt the same definition for the distance R as for the Mg case (vide supra). Similar to Mg, the MEP connecting the $Ca^{2+}(H_2O)_n$ with the $Ca^{2+}(H_2O)_{n-1} + H_2O$ is smooth when no hydrogen-bonded intermediates are formed (see the solid lines with the filled symbols in Figs. 4, 5). The formation of the hydrogen-bonded intermediate results in an energy lowering and alters the MEPs for $R > 3$ Å (dashed line

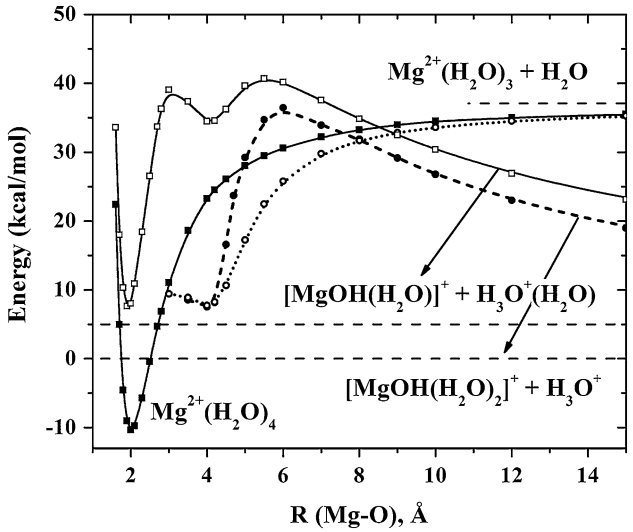

Fig. 3 Minimum energy paths of the $[Mg(H_2O)_4]^{2+}$ system. The *dashed line* with the *filled circles* dissociates to $[MgOH(H_2O)_2]^+ + H_3O^+$, whereas the *solid line* with the *open squares* to $[MgOH(H_2O)]^+ + H_3O^+(H_2O)$

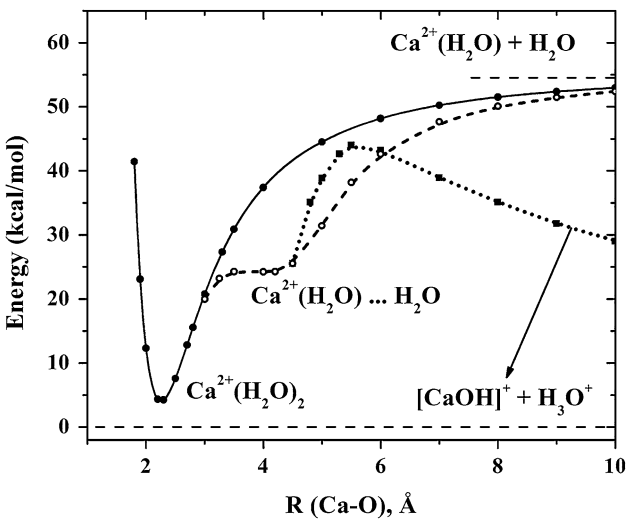

Fig. 4 Minimum energy paths of the $[Ca(H_2O)_2]^{2+}$ system. The *dotted line* with the *filled squares* dissociates to $[CaOH]^+ + H_3O^+$

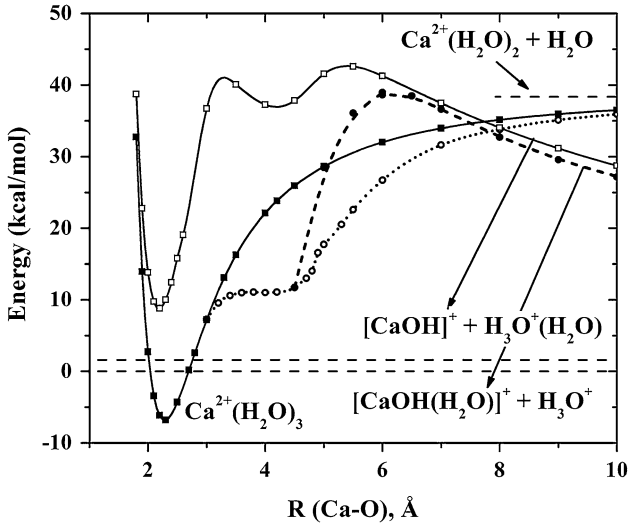

Fig. 5 Minimum energy paths of the $[Ca(H_2O)_3]^{2+}$ system. The *dashed line* with the *filled circles* dissociates to $[CaOH(H_2O)]^+ + H_3O^+$, whereas the *solid line* with the *open squares* to $[CaOH]^+ + H_3O^+(H_2O)$

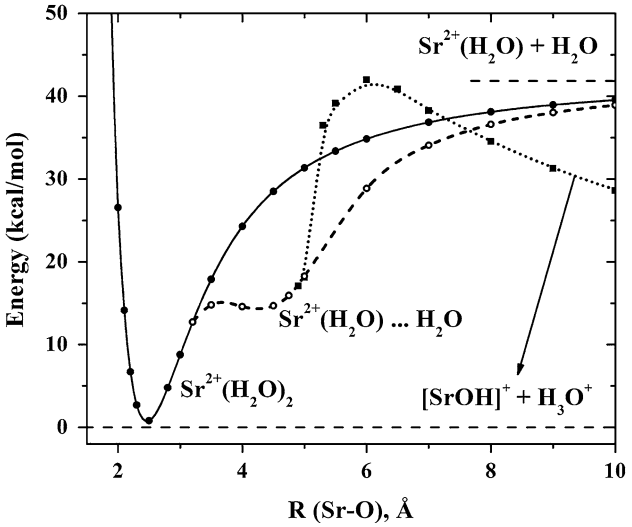

Fig. 6 Minimum energy paths of the $[Sr(H_2O)_2]^{2+}$ system. The *dotted line* with the *filled squares* dissociates to $[SrOH]^+ + H_3O^+$

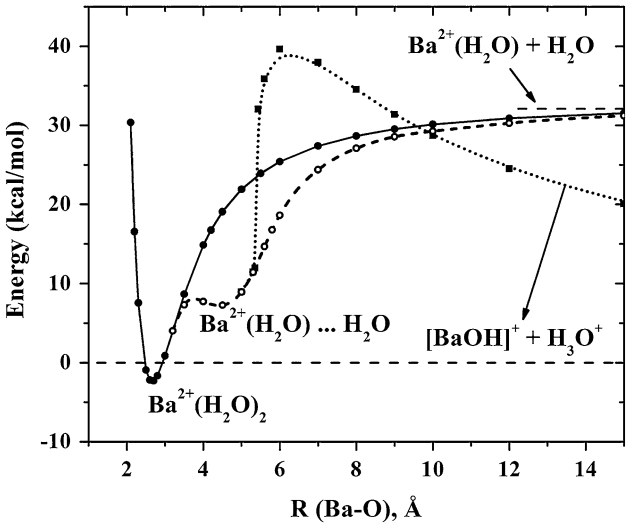

Fig. 7 Minimum energy paths of the $[Ba(H_2O)_2]^{2+}$ system. The *dotted line* with the *filled squares* dissociates to $[BaOH]^+ + H_3O^+$

with open circles in Fig. 4 and dotted line with open circles in Fig. 5).

The $Ca^{2+}(H_2O)\ldots H_2O$ hydrogen-bonded complex can further dissociate via two different paths: an endothermic one leading to $Ca^{2+}(H_2O) + H_2O$ and an exothermic one to $[CaOH]^+ + H_3O^+$ overcoming a barrier of 19.7 kcal/mol. This energy barrier is at least twice as much as the one for the Mg case (8.7 kcal/mol). The difference between the energy levels of $Ca^{2+}(H_2O)_2$ and $[CaOH]^+ + H_3O^+$ is 5.0 kcal/mol, very similar to that for Mg.

As regards the $Ca^{2+}(H_2O)_2\ldots H_2O$ hydrogen-bonded intermediate, it can follow three different routes to dissociation. The first one to $Ca^{2+}(H_2O)_2 + H_2O$ requires an energy of 25.5 kcal/mol, while the other two leading to the hydronium or Zundel-cation loss are exothermic by roughly the same amount, 11.0 and 9.5 kcal/mol, albeit with rather large energy barriers, 27.6 and 33.8 kcal/mol, respectively. The former barrier height is larger than that of Mg (17.0 kcal/mol), whereas the latter one is smaller than the one for Mg (42.7 kcal/mol). The Zundel-cation channel loss proceeds via the $[Ca(H_2O)]^{2+}\ldots H_2O\ldots H_2O$ intermediate (solid line with open squares in Fig. 5), which lies 43.5 kcal/mol above the $Ca^{2+}(H_2O)_3$ global minimum. Our relative energetics are in agreement with the ZPE-corrected DFT values of Peschke et al. [28], Beyer et al. [29], and Carl and Armentrout [16].

3.3 $[Sr(H_2O)_{2,3}]^{2+}$ and $[Ba(H_2O)_{2,3}]^{2+}$

For the Sr and Ba dications, we first examine the cases with two water molecules, the MEPs of which are shown in Figs. 6 and 7. The stationary points of these MEPs have been previously reported by Beyer et al. [29] and Carl et al. [14] at the DFT level of theory with the B3LYP functional. The energy differences between $Sr^{2+}(H_2O)_2$ and $Sr^{2+}(H_2O)\ldots H_2O$ (H-bonded intermediate) and between $Sr^{2+}(H_2O)\ldots H_2O$ and the transition state to $Sr^+(OH) + H_3O^+$ are 13.8 (vs. 13.5 [29], 13.6 [14]) kcal/mol and 27.4 (vs. 23.2 [29], 24.1 [14]) kcal/mol. The corresponding values for Ba are 9.6 (vs. 9.5 [29]) and 32.3 (vs. 29.2 [29]) kcal/mol. The H-bonded intermediate was found to be stabilized monotonically from Mg to Ba with respect to the global $M^{2+}(H_2O)_n$ minimum, while the barrier to the dissociation to hydronium increases from Mg to Ba. However, the final dissociation energy from the equilibrium aqueous

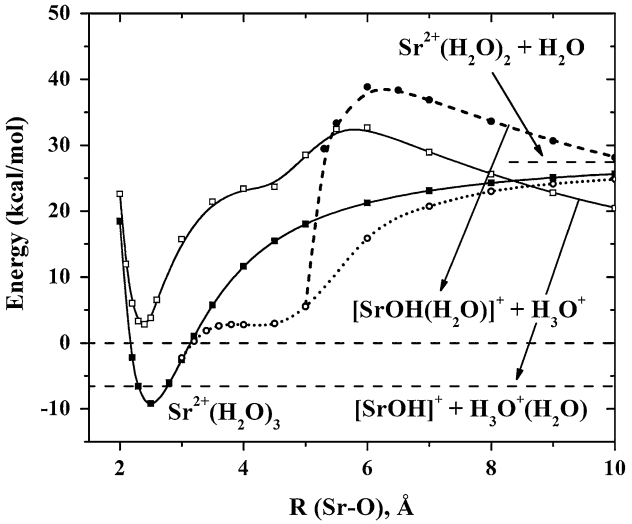

Fig. 8 Minimum energy paths of the $[Sr(H_2O)_3]^{2+}$ system. The *dashed line* with the *filled circles* dissociates to $[SrOH(H_2O)]^+ + H_3O^+$, while the *solid line* with the *open squares* to $[SrOH]^+ + H_3O^+(H_2O)$

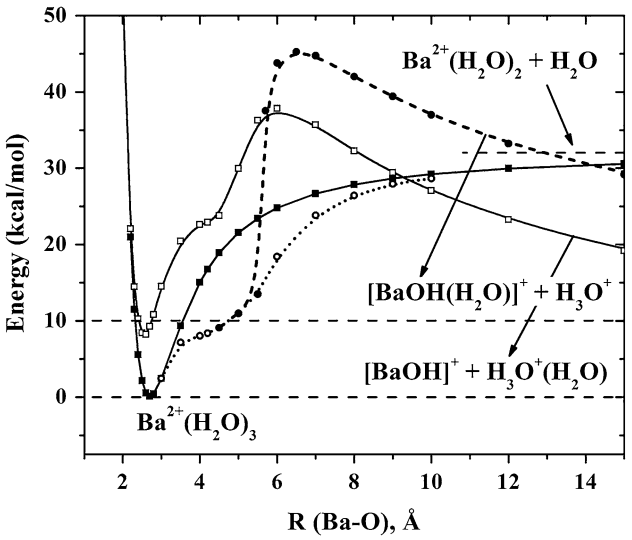

Fig. 9 Minimum energy paths of the $[Ba(H_2O)_3]^{2+}$ system. The *dashed line* with the *filled circles* dissociates to $[BaOH(H_2O)]^+ + H_3O^+$, while the *solid line* with the *open squares* to $[BaOH]^+ + H_3O^+(H_2O)$

complex to the hydronium products remains small within the range of ±5 kcal/mol.

Similar trends are observed for the tri-coordinated aqueous metal clusters. The respective MEPs are depicted in Figs. 8 and 9, and to the best of our knowledge, there is no previous reference regarding their stationary points in the literature. Briefly, the $M^{2+}(H_2O)_3$ minimum lies 12.0/8.4 kcal/mol (M = Sr/Ba) below the $M^{2+}(H_2O)_2\ldots H_2O$ intermediate (albeit not a real minimum for Ba), which in turn is 26.1/24.4 kcal/mol below the water loss asymptote. The transition from $M^{2+}(H_2O)_2\ldots H_2O$ to the $MOH(H_2O)]^+ + H_3O^+$ asymptote proceeds over a barrier of 36.0/42.6 kcal/mol, while the channel leading to $MOH^+ + H_3O^+(H_2O)$ proceeds via a smaller energy barrier (29.8/29.6 kcal/mol) and is associated with a larger exothermicity (9.6/8.2 kcal/mol).

When going from Mg^{2+} to Ba^{2+}, the ionic radii increase and consequently the charge density decreases along this direction, therefore weakening the interaction between $M^{2+}(H_2O)_2$ and H_2O. Consequently, the binding energy is expected to become smaller going from Mg to Ba in complete agreement with Figs. 2, 5, 8, and 9. In addition, the H-bonded $M^{2+}(H_2O)_2\ldots H_2O$ intermediate energetically approaches the equilibrium $M^{2+}(H_2O)_3$ structure at the same time decreasing the already small barrier between those two stationary points. Indeed, according to Fig. 9, this transition for Ba is barrierless, and the $Ba^{2+}(H_2O)_2\ldots H_2O$ "intermediate" is not a local minimum. The case is exactly the same for the "doubly" H-bonded intermediate, $M^{2+}(H_2O)\ldots H_2O\ldots H_2O$, which is 57.1 kcal/mol higher than the $M^{2+}(H_2O)_3$ minimum for Mg and decreases to 46.1, 32.6, and 22.9 kcal/mol for Ca, Sr, and Ba, respectively. The barrier from the former to the latter structure is also decreasing and it actually vanishes for Sr and Ba. A final remark has to do with the relative order of the hydronium and Zundel-cation fragments: For Mg, the hydronium loss channel produces fragments that are lower in energy by 16.3 kcal/mol. On the other hand, Ba prefers the Zundel-cation loss process by 10.0 kcal/mol; Ca and Sr are somewhere in-between.

4 Energetics of the channels corresponding to the water, hydronium, and Zundel-cation loss

In this section, we report the energetics of reactions (1), (2), and (3) as a function of both the metal atom M and the number *n* of water molecules in the cluster. The absolute energies and geometric structures of all molecular species involved in this section are reported in the Supporting Information. Setting as zero of the energy scale, the energy of the $M^{2+}(H_2O)_n$ minima, the energies of the products of reactions (1), (2), and (3) are listed in Table 1. Besides our own values, we also include available theoretical and experimental ones from the literature for reaction (1). The available data for reaction (2) are limited in the literature to the smallest clusters and have already been discussed earlier. We are not aware of any data related to reaction (3) previously reported in the literature.

In Table 1, we list our MP2 results using two different basis sets of double- and triple-ζ quality (MP2/ADZ and MP2/ATZ, see Sect. 2). In general, the two basis sets give values differing no more than a couple of kcal/mol in the

Table 1 Energy differences (kcal/mol) between the $M^{2+}(H_2O)_n$ minima (set as the zero of the energy scale) and the asymptotes corresponding to the unimolecular water loss $M^{2+}(H_2O)_{n-1} + H_2O$, the hydronium loss $[MOH(H_2O)_{n-2}]^+ + H_3O^+$, and the Zundel-cation loss $[MOH(H_2O)_{n-3}]^+ + H_3O^+(H_2O)$ channels, M = Mg, Ca, Sr, Ba and n = 1–6

n	MP2/ADZ	MP2/ATZ[a]	Theory[b]	Expt.[c]	MP2/ADZ	MP2/ATZ[a]	MP2/ADZ	MP2/ATZ[a]
		$[Mg(H_2O)_{n-1}]^{2+} + H_2O$			$[Mg(H_2O)_{n-2}(OH)]^+ + H_3O^+$		$[Mg(H_2O)_{n-3}(OH)]^+ + H_3O^+(H_2O)$	
1	77.9	78.7 (76.8)	78.3					
2	69.6	69.8 (67.6)	69.5		−4.7	−5.3 (−7.3)		
3	56.9	57.3 (54.9)	56.9	53.3 (3.0)	2.3	2.0 (−0.4)	18.5	17.9 (14.1)
4	46.8	46.8 (44.4)	46.2	42.4 (2.5)	10.0	9.7 (7.8)	15.3	14.7 (10.5)
5	32.8	32.4 (29.4)	31.6	27.7 (2.1)	11.1	10.4 (8.0)	9.0	8.0 (3.6)
6	30.7	30.3 (27.8)	24.9	23.3 (1.8)	19.1	18.3 (15.6)	8.0	6.6 (2.3)
		$[Ca(H_2O)_{n-1}]^{2+} + H_2O$			$[Ca(H_2O)_{n-2}(OH)]^+ + H_3O^+$		$[Ca(H_2O)_{n-3}(OH)]^+ + H_3O^+(H_2O)$	
1	58.1	57.1 (55.3)			53.9			
2	50.7	49.9 (47.9)	47.1	49.6 (4.2)	−5.1	−8.2 (−8.8)		
3	46.6	45.2 (43.0)	43.0	40.6 (2.1)	6.2	4.1 (3.3)	7.8	2.9 (0.6)
4	41.8	40.3 (38.6)	37.3	33.7 (2.1)	15.6	13.8 (13.3)	14.4	10.3 (8.4)
5	33.7	32.6 (30.3)	30.6	26.8 (1.8)	19.8	18.2 (17.3)	15.5	12.3 (10.0)
6	30.6	30.3 (28.5)	25.3	23.5 (2.1)	24.5	25.1 (24.4)	16.6	14.4 (12.2)
		$[Sr(H_2O)_{n-1}]^{2+} + H_2O$			$[Sr(H_2O)_{n-2}(OH)]^+ + H_3O^+$		$[Sr(H_2O)_{n-3}(OH)]^+ + H_3O^+(H_2O)$	
1	46.5	48.2 (46.6)	48.1	48.2 (1.4)				
2	40.6	41.7 (39.9)	43.1	41.0 (1.2)	−1.8	−5.6 (−6.4)		
3	38.1	39.1 (37.3)	39.0	34.4 (1.2)	8.7	5.7 (5.0)	2.6	−0.5 (−2.5)
4	33.9	34.3 (32.7)	35.2	29.7 (1.2)	16.4	13.9 (13.7)	8.9	5.8 (4.1)
5	28.9	28.7 (26.5)	29.3	24.4 (0.9)	21.2	18.4 (17.7)	11.6	8.5 (6.6)
6	26.8	26.5 (24.7)	26.8	22.4 (0.7)	26.1	23.8 (23.5)	14.3	10.8 (8.9)
		$[Ba(H_2O)_{n-1}]^{2+} + H_2O$			$[Ba(H_2O)_{n-2}(OH)]^+ + H_3O^+$		$[Ba(H_2O)_{n-3}(OH)]^+ + H_3O^+(H_2O)$	
1	38.9	41.0 (39.5)	41.3					
2	33.8	35.3 (33.6)	37.2		1.0	−5.0 (−6.1)		
3	32.8	33.9 (32.3)	33.7		10.1	5.5 (5.1)	0.0	−5.2 (−7.4)
4	29.1	29.8 (28.4)	30.5	25.6 (0.9)	16.0	12.9 (13.2)	5.5	1.2 (−0.1)
5	25.3	25.3 (23.5)	26.2	21.1 (0.6)	19.8	17.1 (17.6)	7.6	4.1 (3.2)
6	23.0	23.3 (21.8)	23.9	17.9 (0.6)	23.3	21.6 (22.6)	9.0	6.3 (5.8)

[a] ZPE-corrected values are given in parentheses

[b] *Ab initio* values from the literature. Values for Mg and Ca are from Ref. 33 (MP2/6-311 ++G(3d,3p)//MP2/6-311 ++G(3,3)), while values for Sr and Ba are from Ref. 23 (MP2/6-31 + G*//RHF/6-31 + G*)

[c] Experimental hydration enthalpies from the literature. Mg values from Ref. 17 (CID), Ca values from Ref. 16 (CID), Sr values from Ref. 14 (CID), and Ba values from Ref. 5 (BIRD). Uncertainties are reported in parentheses

water loss channel for all four metals; our results are in agreement with previous MP2 calculations with different basis sets. The value of 24.9 kcal/mol for the Mg case with $n = 6$ given by Ref. [33] differs appreciably from our 30.7 and 30.3 kcal/mol values. Our numbers agree, however, better with the 28.5 kcal/mol value of Ref. [23] at the MP2/6-311 + G* level of theory. Our ZPE uncorrected energy differences are always larger than the experimental hydration energies (see Table 1), as expected, but there is better agreement when ZPE is included. Especially for the smaller clusters, our ZPE-corrected values are within the experimental error. For larger clusters, the difference between our values and experiment is of the order of 2–3 kcal/mol and it is due to the fact that our calculations are still missing some portion of electron correlation.

The two channels described by reactions (2) and (3) involve the mono-hydroxides of the four metals under consideration and the hydronium or the hydrated hydronium (Zundel) cations. An interesting observation is the lowering of the energy difference between $M^{2+}(H_2O)_n$ and the

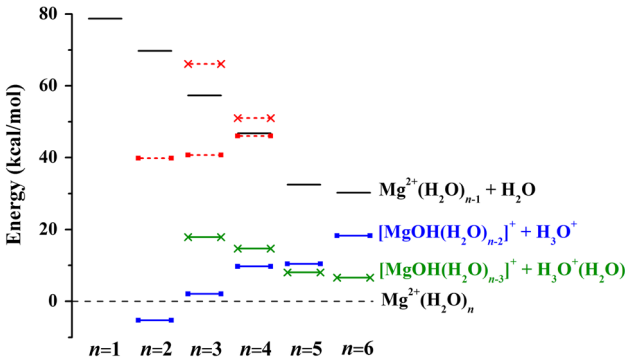

Fig. 10 Relative energies of the $[Mg(H_2O)_n]^{2+}$ (*dashed line* at zero energy), $[Mg(H_2O)_{n-1}]^{2+} + H_2O$ (plain *solid lines*), $[MgOH(H_2O)_{n-2}]^{+} + H_3O^{+}$ (*solid lines* with *filled squares*), and $[MgOH(H_2O)_{n-3}]^{+} + H_3O^{+}(H_2O)$ (*solid lines* with cross symbols) species. The *dashed lines* with the *filled square* symbols correspond to the barriers of the hydronium loss channel and the *dashed lines* with the cross symbols to the barriers of the Zundel-cation loss channel

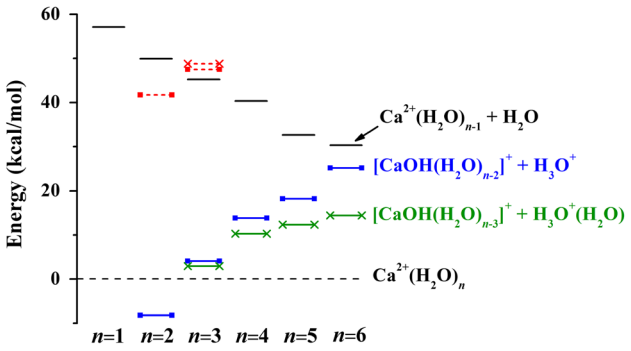

Fig. 11 Similar to Fig. 10, but for Ca

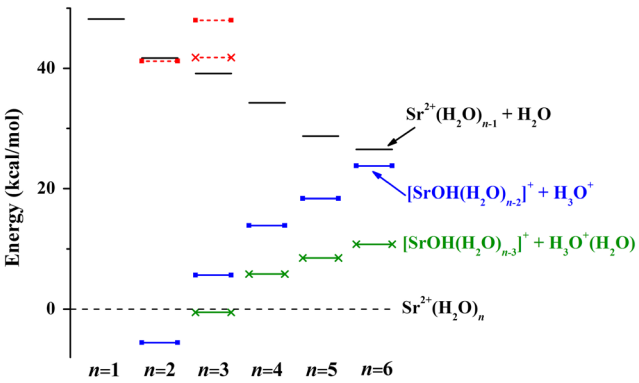

Fig. 12 Similar to Fig. 10, but for Sr

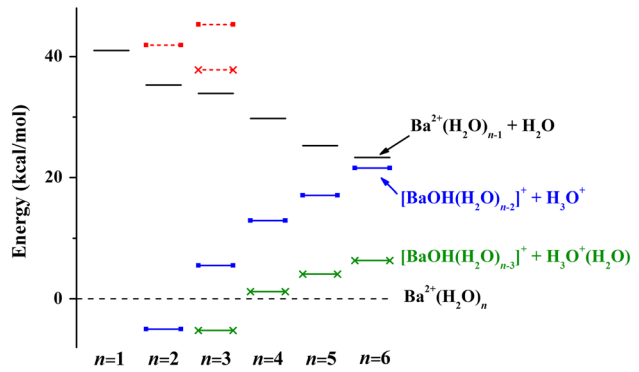

Fig. 13 Similar to Fig. 10, but for Ba

asymptotes of the two channels going from the ADZ to the ATZ basis sets. This holds true for all four metals, and it can be up to 5.2 kcal/mol for the $Ba^{2+}(H_2O)_n \rightarrow [Ba(OH)]^{+} + H_3O^{+}(H_2O)$ energy difference. A similar conclusion was previously noted by Rao et al. [33] for similar systems: "An increase in the quality of the basis set from double-ζ to triple-ζ has a significant effect on the sequential binding energies, irrespective of the geometries used."

Figures 10, 11, 12 and 13 display pictorially the MP2/ATZ results of Table 1. The x axis traces the number n of the water molecules while the y axis the relative energy (kcal/mol). In those figures, the dashed lines correspond to the energy of the $M^{2+}(H_2O)_n$ minima (set as the zero of the energy scale), the plain solid lines to the products of the water loss reaction (1), the solid lines with the closed squares indicate the hydronium loss reaction (2), the dashed lines with the filled squares indicate the barrier height going from the reactants to the products of reaction (2), and finally, the solid and dashed lines with the "×" symbol pertain to the products and the transition state of the Zundel-cation loss reaction (3), respectively. The barrier heights are taken from Figs. 1, 2, 3, 4, 5, 6, 7, 8, and 9 at the MP2/ADZ level of theory. The various asymptotes are also listed on the right hand side of Figs. 10, 11, 12, and 13. In general, the trends with n shown in Figs. 10, 11, 12, and 13 are similar for all metals, except for the channel described by reaction (3) for Mg (shown with the solid lines with the "×" symbol) that crosses the one described by reaction (2) between $n = 4$ and 5. We will discuss the origin of this difference in the subsequent Sect. 5.

It is clear that the water loss channel is endothermic for every possible case of M and value of n. Note that this channel is, as expected, less endothermic for large n values since the insertion of a water molecule to the larger ion–water complexes causes additional steric repulsion. Additionally, for the same value of n, the water loss channel follows a monotonic decrease in the binding energy of the complex going from Mg to Ba. The reason is that all four metals bear the same charge but have a different ionic radius. For instance, the charge density on Ba^{2+} is smaller than that of Mg^{2+} due to its larger size. Therefore, the "affinity" between Ba^{2+} and water is smaller.

The two other channels are competitive for Mg and Ca, whereas for Sr and Ba, the Zundel loss channel produces more stable products (for $n \geq 3$). However, the hydronium and Zundel-cation loss fragments are more difficult to

observe experimentally. The reason that the water loss channel is almost exclusively observed experimentally can be mainly attributed to the large energy barriers that need to be surmounted in order to produce the fragments described by reactions (2) and (3). Specifically, for Mg, the ground-state products $[Mg(OH)(H_2O)_{n-2}]^+ + H_3O^+$ for $n = 2$, 3, and 4 are lower by at least 40 kcal/mol from the $Mg^{2+}(H_2O)_{n-1} + H_2O$ asymptote (see Fig. 10). For $n = 4$, however, the barrier height is comparable to the dehydration energy, and therefore, the two channels described by reactions (1) and (2) are competitive. Judging from the trends observed for $n = 1$–3, we expect the barrier heights to be larger than the dissociation energy to neutral water for larger n. Consequently, the highest number for reaction (2) to be observed is $n = 4$, in complete agreement with the experimental observations [7]. Following the same premise and noting that the energy barriers follow an increasing trend as n goes from 2 to 3 (Figs. 11, 12, 13), we can speculate that the cluster size for the reactions (2) and (3) to occur are $n = 2$ for Ca, Sr, and Ba. The only case where the Zundel cation can appear for Ca, Ba, or Sr is for $n = 3$. More accurate predictions necessitate the calculation of the transition states for larger n values, also including ZPE corrections.

Observe that the energy difference between the two charge separation channels (hydronium and Zundel-cation loss reactions) is bigger for larger clusters and for heavier metal cations. For the same reasons discussed earlier, the binding energy of a single water molecule to a $[MOH(H_2O)_n]^+$ cluster is decreasing with increasing n and atomic number of the metal. Hence, a water molecule prefers (when n or the atomic number increase) to stay more attached to H_3O^+ with a binding energy of 33.7 kcal/mol (at MP2/ATZ) rather than to $[MOH(H_2O)_n]^+$.

5 Mono-hydroxide $[M(H_2O)_n(OH)]^+$ clusters

In this section, we examine the case of the mono-hydroxide water complexes of the titled metal dications, $[MOH(H_2O)_n]^+$. We specifically report the energy needed to detract a water molecule from these species (see Table 2). Additionally, for the case of $n = 2$, we constructed the corresponding MEPs (see Fig. 14). It is shown that for $n = 2$ the lowest energy path is the plain water loss channel and that the products of the hydronium loss process, $M(OH)_2 + H_3O^+$, are much higher in energy.

In Table 2, we list the dissociation energies of the following reaction:

$$\left[MOH(H_2O)_n\right]^+ \rightarrow \left[MOH(H_2O)_{n-1}\right]^+ + H_2O. \quad (4)$$

Similar to the case of the $M^{2+}(H_2O)_n$ clusters, the dissociation energy is a decreasing function of both n and the ionic radii. Namely, it is larger for Mg, which has the smallest ionic radius, and smaller for Ba. It is also larger for $n = 1$ and smaller for $n = 4$. Interestingly, the range of the binding energies, i.e., the difference between the $n = 1$ and $n = 4$ cases, is larger for Mg (27.6 kcal/mol), decreasing to 9.6 (Ca), 6.8 (Sr), and 4.5 (Ba) kcal/mol. In general, we observe smaller differences between the results with the ADZ and ATZ basis sets than for the case of the $M^{2+}(H_2O)_n$ clusters. Our ATZ results for Ba are in agreement with the CCSD(T) results of Ref. [18], while

Table 2 Water detachment energies (kcal/mol) corresponding to the reaction $[MOH(H_2O)_n]^+ \rightarrow [MOH(H_2O)_{n-1}]^+ + H_2O$, M = Mg, Ca, Sr, Ba and $n = 1$–4

n	MP2/ADZ	MP2/ATZ[a]	Theory[b]	MP2/ADZ	MP2/ATZ[a]	Theory[b]
		Mg			Ca	
1	50.0	50.0 (48.0)	59.1	35.3	33.0 (30.9)	36.7
2	39.1	39.1 (36.3)	46.2	32.5	30.6 (28.6)	34.3
3	31.7	31.7 (29.1)	38.4	29.5	28.2 (26.3)	31.7
4	22.6	22.4 (20.2)	27.8	25.9	23.4 (21.4)	
		Sr			Ba	
1	27.6	27.9 (26.0)		23.7	23.4 (21.1)	23.8
2	26.1	26.0 (24.0)		23.2	22.4 (20.3)	21.4
3	24.1	24.2 (22.4)		21.5	21.1 (19.1)	20.3
4	21.8	21.1 (18.9)		19.5	18.9 (16.8)	

[a] ZPE-corrected values are given in parentheses

[b] *Ab initio* values from the literature: Ref. 22 for Mg (MP4SDTQ/6-31G*//SCF/6-31G*), Ref. 26 for Ca (MP2//SCF, 9s7p3d/(Ca), 6-31G*/(O,H)), and Ref. 18 for Ba (CCSD(T)//DFT/*m*PW1PW91)

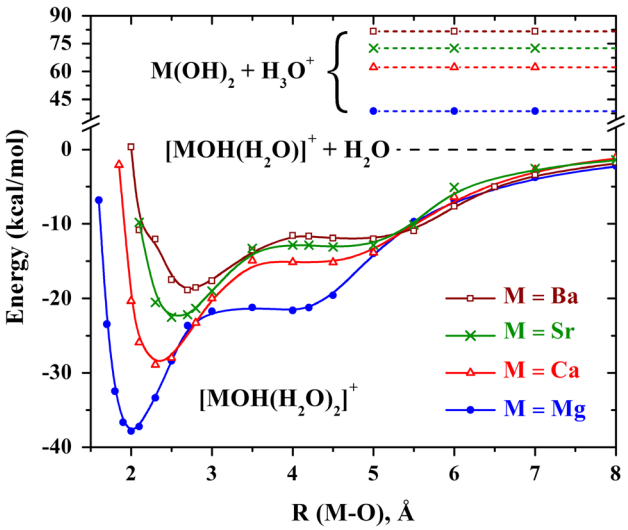

Fig. 14 Minimum energy paths for the $[MOH(H_2O)_2]^+$ clusters, where M = Mg, Ca, Sr, and Ba. The *dashed lines* on the *top* part of the Figure mark the various $M(OH)_2 + H_3O^+$ asymptotes

they differ more than 5 kcal/mol for Mg from the MP4SDTQ results of Ref. [22]. The MP2 results from Ref. [26] for Ca are in good agreement with ours.

It is noteworthy that a water molecule binds stronger to $M^{2+}(H_2O)_{n+1}$ compared to $[MOH(H_2O)_n]^+$ (see Tables 1, 2) due to the stronger Coulombic interaction with a doubly charged metal core. The suggested [24, 29] electronic structure $M^{2+}(H_2O)_n(OH^-)$ indicates the same charge–dipole interaction between the additional water and the metal center for the two systems. However, the negatively charged OH^- group can cause the opposite effect by reducing the binding energy.

The results of Table 2 further explain the qualitative difference seen in the trend of the energetics of channel (3) for Mg (indicated by the solid lines with the "×" symbol in Fig. 10) when compared to the rest of the metals (Figs. 11, 12, 13). The energy levels of reaction channel (3) cross the ones for channel (2) between $n = 4$ and 5 for Mg, whereas for all other metals, there is no such crossing. The reason is that the $[MOH(H_2O)_n]^+$ water detachment energies for the Mg $n = 1$ and 2 clusters (cf. Table 2) are larger than the hydronium–water interaction energy (33.7 kcal/mol at MP2/ATZ), whereas for all other metals, they are smaller than this value, and therefore, the energy levels for channel (3) always lie below the ones for channel (2) for Ca, Sr, and Ba.

In Fig. 14, we show the MEPs corresponding to the removal of one water molecule from $[MOH(H_2O)_2]^+$. These MEPs are constructed by fixing the distance between the metal and the oxygen of the departing water molecule at different lengths and optimizing all other geometrical parameters. After a plateau of width larger than 1 Å for distances $R > 3$ Å, the MEPs converge smoothly to the $[MOH(H_2O)]^+ + H_2O$ asymptote. The aforementioned plateau is caused by the hydrogen bond between the water that is attached to the metal and the one that is departing. The energy of the fragments $M(OH)_2 + H_3O^+$ is shown with dashed lines for the various metals and ranges from ~38 kcal/mol (Mg) to ~78 kcal/mol (Ba) above the $[MOH(H_2O)]^+ + H_2O$ lowest energy asymptote.

The hydration energy of 33.7 kcal/mol (MP2/ATZ) for H_3O^+ is generally larger (except for Mg and $n = 2$) than the binding energy of a water to $[MOH(H_2O)_{n-1}]^+$ indicating that the $M(H_2O)_{n-3}(OH)_2 + H_3O^+(H_2O)$ fragments will be closer in energy to the $[MOH(H_2O)_{n-1}]^+ + H_2O$ ones. Therefore, the possibility exists for $[MOH(H_2O)_n]^+$ ($n \geq 3$) to dissociate to $M(H_2O)_{n-3}(OH)_2 + H_3O^+(H_2O)$, especially for Ba and large n. The Supporting Information includes the geometries and energies of the $M(OH)_2$ molecules as well as the energy required to detach a hydroxide from $[M(H_2O)_n(OH)]^+$, i.e., the dissociation energies for the $[M(H_2O)_n(OH)]^+ \rightarrow [M(H_2O)_n]^{2+} + OH^-$ reaction.

6 Synopsis

We examined the MEPs along which a water molecule can be detached from the pure and mono-hydroxide water complexes of the alkaline earth metals Mg^{2+}, Ca^{2+}, Sr^{2+}, and Ba^{2+}. Three different channels were investigated: one leading to the unimolecular water loss and two leading to the loss of a hydronium and a Zundel (singly hydrated hydronium) cation. For the cases with two, three, and four (only for Mg) water molecules, we constructed MEPs at the MP2/ADZ level of theory, while for the larger systems, we investigated only the reactants and products of the above three processes at the MP2/ATZ level. In the case of the mono-hydroxide compounds, we report the MEPs for the systems with two water molecules and the energetics with up to four water molecules.

Despite the voluminous work reported in the literature for the systems studied presently, this is the first systematic work encompassing all four metals with up to six water molecules and three dissociation channels. Our results are consistent with several experimental observations, such as the fact that only the small clusters dissociate to fragments involving the hydronium cation. Additionally, we propose the possibility of the production of the Zundel cation for the heavier metals with three water molecules. The large energy barriers of the charge separation channels for the largest complexes prevent them from being observed, although they are more exothermic than the water loss ones. Finally, mono-hydroxide water clusters prefer the pure water loss channel, because it is energetically more favorable.

Acknowledgments We acknowledge useful discussions with Drs. Nikolai Petrik and Gregory Kimmel of PNNL. This work was supported by the US Department of Energy, Office of Basic Energy Sciences, Division of Chemical Sciences, Geosciences and Biosciences. Pacific Northwest National Laboratory (PNNL) is a multiprogram national laboratory operated for DOE by Battelle. This research used resources of the National Energy Research Scientific Computing Center, which is supported by the Office of Science of the US Department of Energy under Contract No. DE-AC02-05CH11231.

References

1. Spears KG, Fehsenfeld FC (1972) J Chem Phys 56:5698
2. Blades AT, Jayaweera P, Ikonomou MG, Kerbale P (1990) J Chem Phys 92:5900
3. Peschke M, Blades AT, Kerbale P (1998) J Phys Chem A 102:9978
4. Pye CC, Rudolph WW (1998) J Phys Chem A 102:9933
5. Rodriguez-Cruz SE, Jockush RA, Williams ER (1999) J Am Chem Soc 121:8898
6. Barran PE, Walker NR, Stace AJ (2000) J Chem Phys 112:6173
7. Shvartsburg AA, Michael Sin KW (2001) J Am Chem Soc 123:10071

8. Markham GD, Glusker JP, Bock CW (2002) J Phys Chem B 106:5118
9. Wong RL, Paech K, Williams ER (2004) Int J Mass Spectrom 232:59
10. Bush MF, Saykally RJ, Williams ER (2007) Chem Phys Chem 8:2245
11. Carl DR, Moison RM, Armentrout PB (2007) Int J Mass Spectrom 265:308
12. Carl DR, Moison RM, Armentrout PB (2009) J Am Soc Mass Spectrom 20:2312
13. Bush MF, O'Brien JT, Prell JS, Wu C-C, Saykally RJ, Williams ER (2009) J Am Chem Soc 131:13270
14. Carl DR, Chatterjce BK, Armentrout PB (2010) J Chem Phys 132:044303
15. Cabavillas-Vidosa I, Rossa M, Pino GA, Ferrero JC, Cobos CJ (2012) Phys Chem Chem Phys 14:4276
16. Carl DR, Armentrout PB (2012) J Phys Chem A 116:3802
17. Carl DR, Armentrout PB (2013) Chem Phys Chem 14:681
18. Cabavillas-Vidosa I, Rossa M, Pino GA, Ferrero JC, Cobos CJ (2013) J Phys Chem A 117:4997
19. Kaupp M, Schleyer PR (1992) J Phys Chem 96:7316
20. Klobukowski M (1992) Can J Chem 70:589
21. Bauschlicher CW Jr, Sodupe M, Partridge H (1992) J Chem Phys 96:4453
22. Watanabe H, Iwata S, Hashimoto K, Misaizu F, Fuke K (1995) J Am Chem Soc 117:755
23. Glendening ED, Feller D (1996) J Chem Phys 100:4790
24. Kaufman Katz A, Glusker JP, Beebe SA, Bock CW (1996) J Am Chem Soc 118:5752
25. Markham GD, Glusker JP, Bock CL, Trachtman M, Bock CW (1996) J Chem Phys 100:3488
26. Watanabe H, Iwata S (1997) J Phys Chem A 101:487
27. Pavlov M, Siegbahn EM, Sandström M (1998) J Phys Chem A 102:219
28. Peschke M, Blades AT, Kebarle P (1999) Int J Mass Spectrom 185/186/187:685
29. Beyer M, Williams ER, Bondybey VE (1999) J Am Chem Soc 121:1565
30. Dudev T, Lim C (1999) J Phys Chem A 103:8093
31. Merrill GN, Webb SP, Bivin DB (2003) J Phys Chem A 107:386
32. Dang LX, Schenter GK, Glezakou VA, Fulton JL (2006) J Phys Chem B110:23644
33. Sirinivasa Rao J, Dinadayalane TC, Leszczynski J, Narahavi Sastry G (2008) J Phys Chem A 112:12944
34. Lei XL, Pan BC (2010) J Phys Chem A 114:7595
35. Gonzalez JD, Florez E, Romero J, Reyes A, Restrepo A (2013) J Mol Model 19:1763
36. Miliordos E, Xantheas SS (2013) Phys Chem Chem Phys. doi:10.1039/c3cp53636j
37. Baes CFJ, Mesmer RE (1986) The hydrolysis of cations. Krieger Publishing Company, Malabar, FA
38. Moore CE (1971) Atomic energy levels as derived from the analysis of optical spectra. COM-72-50283, US Department of Commerce, National Technical Information Service, National Bureau of Standards, Washington, DC
39. Lias SG, Bartmess JE, Liebman JF, Holmes JL, Levin RD, Mallard WG (1988) J Phys Chem Ref Data 17(Suppl 1):1
40. Dunning TH Jr (1989) J Chem Phys 90:1007
41. Kendall RA, Dunning TH Jr, Harrison RJ (1992) J Chem Phys 96:6796
42. Woon DE, Peterson KA, Dunning TH Jr, in preparation, and as implemented in MOLPRO (ref [45])
43. Koput J, Peterson KA (2002) J Phys Chem A 106:9595
44. Lim IS, Stoll H, Schwerdtfeger P (2006) J Chem Phys 124:034107
45. MOLPRO, version 2010.1, a package of ab initio programs, Werner HJ, Knowles PJ, Knizia G, Manby FR, Schütz M, Celani P, Korona T, Lindh R, Mitrushenkov A, Rauhut G, Shamasundar KR, Adler TB, Amos RD, Bernhardsson A, Berning A, Cooper DL, Deegan MJO, Dobbyn AJ, Eckert F, Goll E, Hampel C, Hesselmann A, Hetzer G, Hrenar T, Jansen G, Köppl C, Liu Y, Lloyd AW, Mata RA, May AJ, McNicholas SJ, Meyer W, Mura ME, Nicklass A, O'Neill DP, Palmieri P, Pflüger K, Pitzer R, Reiher M, Shiozaki T, Stoll H, Stone AJ, Tarroni R, Thorsteinsson T, Wang M, Wolf A. http://www.molpro.net
46. Gaussian 09, Revision D.01, Frisch MJ, Trucks GW, Schlegel, HB, Scuseria GE, Robb MA, Cheeseman JR, Scalmani G, Barone V, Mennucci B, Petersson GA, Nakatsuji H, Caricato M, Li X, Hratchian HP, Izmaylov AF, Bloino J, Zheng G, Sonnenberg JL, Hada M, Ehara M, Toyota K, Fukuda R, Hasegawa J, Ishida M, Nakajima T, Honda Y, Kitao O, Nakai H, Vreven T, Montgomery JAJr, Peralta JE, Ogliaro F, Bearpark M, Heyd JJ, Brothers E, Kudin KN, Staroverov VN, Kobayashi R, Normand J, Raghavachari K, Rendell A, Burant JC, Iyengar SS, Tomasi J, Cossi M, Rega N, Millam NJ, Klene M, Knox JE, Cross JB, Bakken V, Adamo C, Jaramillo J, Gomperts R, Stratmann RE, Yazyev O, Austin AJ, Cammi R, Pomelli C, Ochterski JW, Martin RL, Morokuma K, Zakrzewski VG, Voth GA, Salvador P, Dannenberg JJ, Dapprich S, Daniels AD, Farkas Ã, Foresman JB, Ortiz JV, Cioslowski J, Fox DJ (2009) Gaussian, Inc., Wallingford, CT